RSC Advances

PAPER

View Article Online
View Journal | View Issue

Cite this: *RSC Adv.*, 2025, **15**, 38260

DFT mechanistic insights into the atomic layer deposition of β-Ga_2O_3

Jiamin Yang,[a] Yuhang Jing,*[a] Zhiqiang Yang,[a] Junqing Zhao,[a] Weiqi Li,[b] Jihong Yan,[d] Jianqun Yang[c] and Xingji Li*[c]

Ga_2O_3 is a wide bandgap semiconductor material exhibiting vast application potential in power electronics, radio frequency electronics, deep ultraviolet optoelectronic devices, and other fields. The fabrication of β-Ga_2O_3 thin films presents a formidable yet indispensable task although a multitude of epitaxial growth techniques has been utilized, with chemical vapor deposition (CVD) and atomic layer deposition (ALD) being the most prevalent. However, the growth mechanism of β-Ga_2O_3, especially through ALD using trimethyl gallium (TMG) and O_2, is still poorly understood. Thus, in this study, we employ density functional theory (DFT) to investigate the surface reaction mechanisms and detailed pathways of β-Ga_2O_3 ALD with TMG and O_2 as the precursors. The process consists of two self-limiting half-reactions, TMG chemisorption and O_2 oxidation, which collectively enable a layer-by-layer growth. Our computations reveal that the methyl groups in TMG undergo progressive dissociation and hydrogen transfer, ultimately desorbing as stable gaseous products such as CH_4 and C_2H_4. These results provide atomistic insights into the key intermediates and energy barriers governing the ALD process, facilitating a better control over the film properties and offering a general framework for mechanistic studies in metal oxide ALD.

Received 25th July 2025
Accepted 23rd September 2025

DOI: 10.1039/d5ra05380c

rsc.li/rsc-advances

1. Introduction

Gallium oxide (Ga_2O_3) holds an important strategic position in the prospective layout of semiconductor technology due to its excellent physical properties,[1,2] and thus, numerous studies have been conducted on its various crystal forms, such as α-Ga_2O_3,[3,4] β-Ga_2O_3,[5,6] γ-Ga_2O_3,[7] δ-Ga_2O_3[8] and ε-Ga_2O_3, and their applications.[9,10]

Among the different phases of Ga_2O_3, β-Ga_2O_3 is the most stable crystal structure[11] and the only natural substrate that can be grown into large single crystals *via* melt growth.[1] β-Ga_2O_3 exhibits superior electrical properties and thermal stability, with a melting point reaching up to 1900 °C.[14] In contrast, the thermal stability of other polymorphs of Ga_2O_3 are poor, and they convert to the stable β-form upon heat treatment.[12] Furthermore, β-Ga_2O_3 is an ultra-wide bandgap transparent semiconductor oxide with an energy gap of 4.85 eV.[13] Thus, β-Ga_2O_3 is the most widely used phase of gallium oxide in the semiconductor field, including the manufacturing of electronic high-power devices such as power field-effect transistors (FETs) and photodiodes,[14] production of solar-blind UV photodetectors,[11] gas sensors,[15] and other devices. Moreover, it can be used as a catalyst; for instance, β-Ga_2O_3(001) can be used in the adsorption of reactants and intermediates involved in the hydrogenation of CO_2[16] and Ag-loaded β-Ga_2O_3 photocatalysts can be used in the photocatalytic carbon dioxide reduction.[17]

Taken together, these studies suggest that the synthesis of β-Ga_2O_3 thin films is crucial, but it is also challenging. β-Ga_2O_3 films have been grown by epitaxial methods such as metal–organic chemical vapor deposition (MOCVD),[13,18] halide vapor phase epitaxy (HVPE),[19] mist chemical vapor deposition (mist-CVD)[20] and atomic layer deposition (ALD).[21] Owing to the superior thickness control and conformal coverage offered by ALD, it is extensively employed in the microelectronics industry for the deposition of β-Ga_2O_3 films and other films.[11] Thermal ALD, which employs molecular substances, and PEALD, which utilizes active substances in the plasma state as oxidation or reduction reactants, are the predominantly utilized methods of ALD.[21] Through these studies, we found that PEALD can generate high-purity and well uniform Ga_2O_3 thin films at low temperatures,[22–24] with high controllability,[25] and it can also achieve uniform deposition on complex surface structures.[26,27] Thus, researchers have also studied how to apply β-Ga_2O_3 obtained from PEALD in fields such as micro-nano electronic devices, optoelectronic devices, and energy storage devices.[28–31]

[a]*Department of Astronautical Science and Mechanics, Harbin Institute of Technology, Harbin, Heilongjiang 150001, China. E-mail: jingyh@hit.edu.cn*

[b]*School of Physics, Harbin Institute of Technology, Harbin, Heilongjiang 150001, China*

[c]*Technology Innovation Center of Materials and Devices at Extreme Environment, Harbin Institute of Technology, Harbin, Heilongjiang 150001, China. E-mail: lxj0218@hit.edu.cn*

[d]*Laboratory for Space Environment and Physical Sciences, Harbin Institute of Technology, Harbin, Heilongjiang 150001, China*

The previous research on ALD of β-Ga_2O_3 mostly focused on experimental studies. However, experimental research is expensive and has drawbacks such as experimental errors and limitations. Thus, to resolve this, theoretical research methods such as density functional theory (DFT) were employed to understand the underlying chemical mechanisms in the ALD process.[32] In ALD studies on Ga_2O_3 using DFT, they investigated the growth of κ-Ga_2O_3,[33] the catalytic activity of gallium oxide in carbon dioxide hydrogenation reactions,[16] or amorphous gallium oxide thin films deposited on polycrystalline diamond substrates,[5] with no research about the growth of β-Ga_2O_3. However, several researchers have conducted studies on the ALD growth of alumina. For instance, experiments on the growth of alumina,[34] using the *ab initio* method to investigate alumina growth using TMA and O_3, O (atomic oxygen), or H_2O as precursors,[35] and ALD of Al_2O_3 using the DFT method.[36] Despite the fact that certain researchers have investigated the ALD reaction of gallium oxide using trimethylgallium (TMG), which has a similar structure to trimethylaluminum (TMA),[37] the reaction mechanism during the growth process of β-Ga_2O_3 thin films continues to be ambiguous. Therefore, herein, we conducted a study on the ALD of β-Ga_2O_3 using the DFT method to offer insights into designing, analyzing, or enhancing the ALD process in a systematic manner. In previous studies, various researchers chose different precursors for ALD of β-Ga_2O_3.[21] Some opted for TMG and Ar/O_2 plasma,[24,27,38] others preferred TMG and O_3,[23,39] some studies utilized GaI_3 and O_3 as precursors,[40] while others chose $Ga(C_2H_5)_3$ (TEG) and O_2.[41] The high volatility of the precursor can enhance the quality of ALD and enable processing over larger areas, and TMG exhibits a high vapor pressure of 227 Torr at room temperature, making it the preferred choice among various precursors.[39] Consequently, TMG and O_2 are chosen as the precursors in this work.

In this study, we performed DFT calculations to reveal the mechanism for the atomic layer deposition of β-Ga_2O_3 using TMG and O_2 as precursors. Single crystals of β-Ga_2O_3 cleave readily on the (100) plane, which suggests that this is the most stable surface.[42] We selected the (100) plane of β-Ga_2O_3 as the reaction surface, and effective reaction pathways were identified by reducing the bond strength of critical species such as methyl, hydroxyl, and hydrogen atoms. The energy changes in each stable structure were calculated using DFT during the bond energy regulation process, and we elastically deformed molecules along the reaction path while keeping the energy minimum to determine the energy barrier and activation energy. The equilibrium state and activating energy were then analyzed in detail, confirming the feasibility of the reaction method. Through this process, we provide a deep understanding of the reaction mechanism for β-Ga_2O_3 growth.

2. Computational models and methods

All calculations were conducted in the framework of DFT by using the Vienna *ab initio* simulation package (VASP).[43,44] The use of the Perdew, Burke, and Ernzerhof (PBE) exchange correlation functions based on the Projection Augmented Wave (PAW) method can more accurately calculate the electronic structure and properties of materials,[45–47] providing a more reliable theoretical basis for studying material properties. Pseudopotentials were generated with $4s^2$, $4p^1$ valence electrons for gallium and $2s^2$, $2p^4$ for oxygen. The smoothing method and Fermi Dirac distribution function were used in the calculation, with the smoothing width set to 0.2 eV. For all structural optimizations, a plane wave basis set with a cutoff energy of 400 eV was used and the ionic positions were allowed to relax until the forces were less than 0.04 eV $Å^{-1}$. In addition, the climbing image nudged elastic band (CINEB) method was used to obtain a more accurate energy maximum.[48,49]

Ga_2O_3 exhibits several important surface planes, including polar (100) and (001) facets, non-polar (010) and (101) facets, as well as semi-polar surfaces such as (201). The (100) plane of β-Ga_2O_3 was selected for this study given that it is the thermodynamically most stable natural cleavage plane and the most commonly used in power electronic devices.[42] Its unique anisotropic trench-like structure offers diverse active sites for surface chemical reactions, which is crucial for understanding and controlling the surface states and electronic performance of devices.

In this work, the unit cell model used for simulation is monoclinic β-Ga_2O_3 containing 8 Ga atoms and 12 O atoms. A supercell of $1 \times 3 \times 2$ unit cells containing the (100) plane was constructed and optimized. The β-Ga_2O_3 surfaces were modeled by periodic slab models with four Ga layers and seven O layers. This extra O atom layer containing 12 oxygen atoms is located at the bottom of the model and used to artificially passivate floating bonds on the bottom surface by bonding with hydrogen atoms. In addition, the bottom layer was frozen at its bulk position, while other layers were allowed to relax in all calculations. To minimize the artificial interlayer interactions under the periodic boundary condition, periodic boundary conditions were imposed along both the x and y directions for atom movement, and vacuum of 20 Å was added perpendicular to the layer planes of β-Ga_2O_3.[50] The length, width, and height of the simulated crystal cell size are therefore 9.138 Å, 11.632 Å, and 33.6453 Å, respectively. A $2 \times 2 \times 1$ k-point grid was built to perform ALD simulation, where the reactants descend vertically along the (100) direction to the reaction surface in the simulation cell when simulating the deposition process of gallium oxide in this study.

3. Results and discussion

3.1 Reaction mechanism of β-Ga_2O_3 growth

The ALD growth process of β-Ga_2O_3 can be regarded as two alternating addition processes of Ga and O atoms, hereby referred to as reactions A and B, respectively, as shown in Fig. 1. In this work, we chose TMG and O_2 as the precursors to provide Ga and O atoms for this process, respectively. We disregard other non-essential reactions occurring in the gas phase, concentrating instead on how the precursor, upon adsorption onto the surface, retains the target atoms through the reaction,

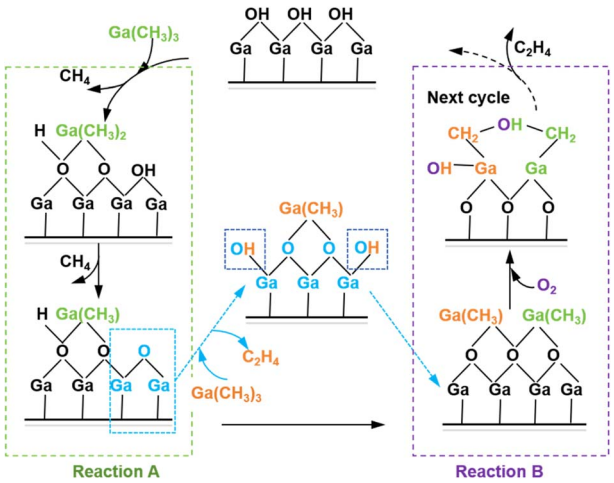

Fig. 1 Main reaction process of β-Ga_2O_3 growth.

while simultaneously expelling surplus atoms *via* gas generation.

In the first half-cycle, hereby referred to as reaction A, $Ga(CH_3)_3$ deposited on the hydrogen-terminated gallium oxide surface reacts with hydroxide radical, and two CH_4 are generated during this process and leave the system in the form of gas, leaving behind methyl gallium on the surface of gallium oxide. During the process of reaction A, the H atom in the surface hydroxyl group reacts with the methyl group to form CH_4, leaving the β-Ga_2O_3 surface with only O atoms. $Ga(CH_3)_3$ is subsequently deposited onto this surface, reacting to produce hydroxyl groups and methyl gallium, which served as reactants for reactions A and B, respectively. Following the deposition reaction, in the second half-cycle, hereby referred to as reaction B, O_2 enters the reaction system and reacts with methyl gallium. The C atom in methyl gallium reacts to form C_2H_4 during this process and leaves the reaction system, leaving hydroxyl on the surface. These hydroxyl groups can react with trimethylgallium again during the next deposition process, forming the ALD cycle, as shown in Fig. 1. β-Ga_2O_3 can continuously grow through this reaction cycle. This work will provide a detailed description of these reaction processes and their mechanisms, including their energy changes and potential barriers.

3.2 Deposition of $Ga(CH_3)_3$ onto the hydrogen-terminated β-Ga_2O_3 surface

We first investigate the reaction and mechanism of $Ga(CH_3)_3$ deposition on the surface of hydrogen-terminated β-Ga_2O_3. The hydrogen-terminated β-Ga_2O_3 model is shown in Fig. 2a. It can be observed that half of the H atoms on the surface are bonded to a single O atom, while the other half is located between two O atoms, forming bridging bonds with both. Furthermore, the bottom layer of atoms in this model was fixed at its bulk positions, while the rest was allowed to relax. At the bottom of the entire model, hydrogen atoms are used to passivate the floating bonds.[42] This reaction process can be summarized by chemical reaction (1). The form of this equation is based on the work by G. Scarel *et al.* on the atomic layer deposition of alumina thin films using O_3 and TMA.[36]

$$2\mathrm{surf-OH} + \mathrm{Ga(CH_3)_3(g)} \rightarrow \mathrm{surf-O} + \mathrm{surf-O-Ga(CH_3)} + 2\mathrm{CH_4} \quad (1)$$

3.2.1 Generation of the first CH_4 gas molecule. We placed $Ga(CH_3)_3$ approximately 3 Å above the surface of hydrogen-terminated gallium oxide, allowing it to deposit onto the surface. Originally, the O atom on the hydrogen-terminated β-Ga_2O_3 surface beneath trimethylgallium was bonded to two H atoms. Upon deposition and bonding of TMG to this oxygen atom, one of its O–H bonds was broken. This hydrogen atom, which was originally part of a bridging hydroxyl group, subsequently formed a new hydroxyl group with a neighboring

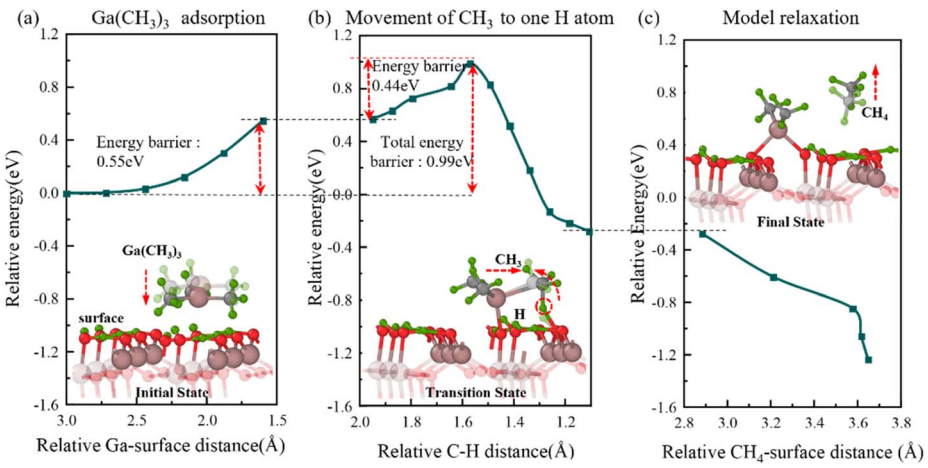

Fig. 2 Semi-transparent and solid structures showing the configurations before and after the reaction step, respectively. The process of $Ga(CH_3)_3$ deposition on hydrogen-terminated gallium oxide to form the first CH_4 gas molecule. (a) Relative energy with distance from trimethylgallium to surface during $Ga(CH_3)_3$ deposition. (b) Relative energy with distance between C and H atoms during the stretching of CH_3 above this nearest surface H atom. (c) Relative energy during the model relaxation.

surface oxygen atom. The relative energy during the deposition progress is shown in Fig. 2a, where the energy barrier for Ga adsorbed on the surface is 0.55 eV. Due to the fact that the coordination number of gallium is four, the Ga atom in $Ga(CH_3)_3$ only binds to one surface O atom. Although no methyl groups decomposed on the surface during the deposition and bonding process, the bond energy between Ga atoms and C atoms diminishes, enabling the Ga atoms to more readily lose CH_3 to them.

Then, to facilitate the reaction between the methyl group and surface H atoms, the distance between Ga atoms and C atoms is increased by moving the methyl group close to the H atom. During this process, the H atoms on the methyl group rotate upwards to provide an adsorption site for the fourth H atom, which generates CH_4. Fig. 2b shows the relative energy with the distance between the moving methyl C atom and the target H atom, where the H atom in the hydroxyl group after the movement forms a bond with the methyl group, and the reaction barrier to overcome during this movement process is 0.44 eV. The relative energy increases and reaches the maximum when this methyl group is moved far enough from the Ga atom and attracts surface H atoms to bond with it, the Ga–C bond breaks and CH_4 is generated after relaxation. When CH_4 is generated, due to the repulsive force between the atoms, the relative energy decreases as the C and H atoms rotate in a new favorable direction. Fig. 2c shows the relative energy during model relaxation.

It can be noticed that the total energy barrier during the deposition of trimethylgallium onto the surface of hydrogen-terminated gallium oxide to generate the first CH_4 is 0.99 eV. Also, there is no energy barrier associated with this process when the model structure relaxes towards its lower energy configuration.

3.2.2 Generation of the second CH_4 gas molecule. Upon the generation of the initial CH_4 and its subsequent departure from the reaction surface, we eliminated it from the model to mimic its detachment from the reaction system post generation. During the subsequent relaxation process, the O atom that was previously bonded with an H atom on the surface near dimethylgallium dissociates from the H atom and forms a bond with the Ga atom within dimethylgallium.

Based on this premise, we first moved another methyl group to the nearest hydrogen atom to weaken the bond energy between the methyl group and the Ga atom, thereby promoting the reaction of the methyl group with the surface. Fig. 3a illustrates the variation in the relative energy with C–H distance during this process, where the energy barrier associated with this move is 0.93 eV. Subsequently, we moved the surface H atom towards the direction of this methyl group to promote the reaction of the H atom with the methyl group, and Fig. 3b shows the variation in relative energy with C–H distance during this process. During this process, the H atoms on the methyl group rotate upwards to provide an adsorption site for the fourth H atom, which generates CH_4. When the H atom breaks the surface O–H bond during its movement towards the methyl group, the relative energy reaches its maximum value, and then the bonding between the H atom and the methyl group is an exothermic process, leading to a reduction in relative energy.

However, CH_4 cannot be generated even after movement because the positions of the Ga and C atoms remain fixed during the movement process. Upon the release of atomic constraints and subsequent model relaxation, the Ga–C bond disintegrates, producing CH_4, which then detaches from the reaction system. Due to the loss of another methyl group from the Ga atom, during the relaxation of the model, the Ga atom can form bond with another O atom. At this time, the Ga atom forms bonds with the three O atoms on the surface. This also causes one O–H bond in the original O–H–O bond of the O atom to break and form a hydroxyl group on the surface, which should facilitate the occurrence of subsequent reactions.

The cumulative energy barrier throughout the entire reaction process in the generation of the second CH_4 is 1.71 eV. The

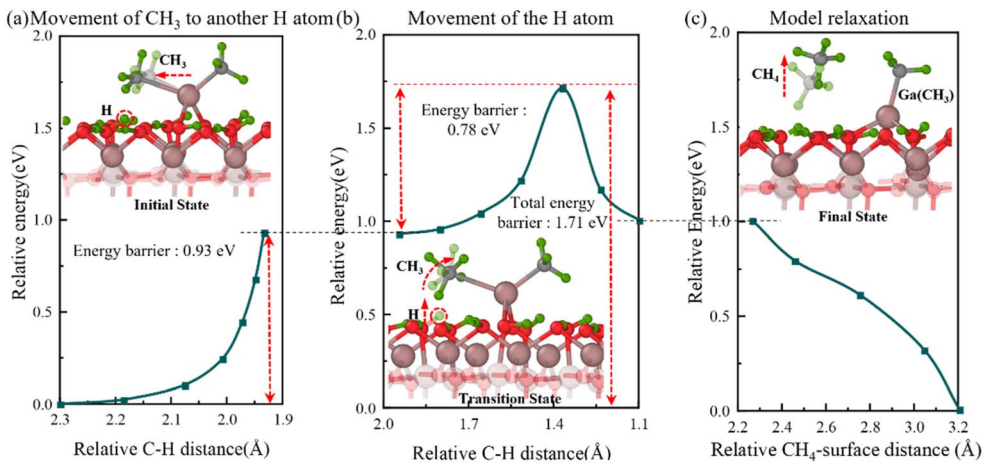

Fig. 3 Semi-transparent and solid structures showing the configurations before and after the reaction step, respectively. Three elementary steps underlying the movement of CH_3 and H atom to form the second CH_4 gas molecule. (a) Relative energy with distance between C and H atoms during the stretching of the second CH_3 over an H atom. (b) Relative energy with distance between C and H atoms during stretching of the H atom towards CH_3. (c) Relative energy during the model relaxation.

model relaxation process, as depicted in Fig. 3c, progressively transforms the non-equilibrium system into a state of decreasing energy equilibrium, with no energy barrier present.

In the above-mentioned reaction of $Ga(CH_3)_3$ deposition (reaction A), Ga atoms form bonds with surface O atoms, thereby remaining on the surface to provide a source of gallium for the growth of β-Ga_2O_3. Also, after the reaction product CH_4 has left the system, the H atoms are taken away from the surface hydroxyl group, leaving behind only O atoms on the surface. The subsequent deposition of trimethylgallium will react with the β-Ga_2O_3 surface with only O atoms, which we will discuss in the subsequent section.

3.3 Deposition of $Ga(CH_3)_3$ onto β-Ga_2O_3 surface with only O atoms

The deposition process of trimethylgallium on the β-Ga_2O_3 surface with only O atoms to produce hydroxyl and C_2H_4 can be represented by chemical reaction (2). This equation is inspired by the research conducted by G Prechtl *et al.*, who investigated the deposition of aluminum oxide atomic layers in high aspect ratio channels using TMA and O_3, O or water.[35]

$$3\mathrm{surf}-\mathrm{O}+\mathrm{Ga(CH_3)_3(g)}\rightarrow 2\mathrm{surf}-\mathrm{OH}+\mathrm{surf}-\mathrm{O}-\mathrm{Ga(CH_3)}+\mathrm{C_2H_4} \quad (2)$$

At the beginning of the reaction, we placed $Ga(CH_3)_3$ approximately 2.5 Å above the surface of gallium oxide. As illustrated in Fig. 4a, all the Ga–C bonds within $Ga(CH_3)_3$ are initially parallel and in the same plane, which is perpendicular to the boundary of the β-Ga_2O_3 simulation cell. Also, the Ga atom in $Ga(CH_3)_3$ is situated between two O atoms on the surface, facilitating its subsequent binding with these O atoms as $Ga(CH_3)_3$ descends vertically and adheres to the gallium oxide surface.

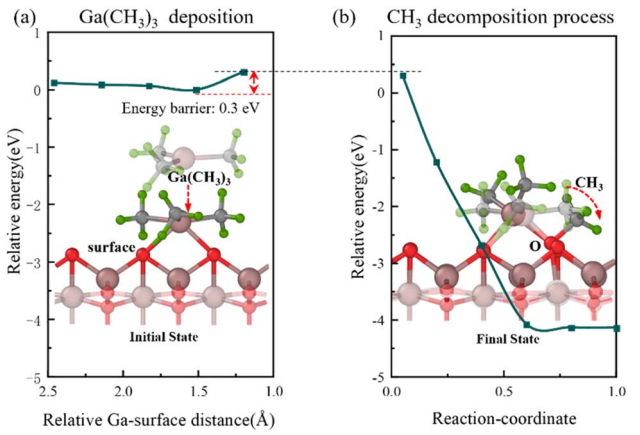

Fig. 4 Semi-transparent and solid structures showing the configurations before and after the reaction step, respectively. $Ga(CH_3)_3$ deposits onto the β-Ga_2O_3 surface with only O atoms. (a) Relative energy with distance between Ga and surface during the $Ga(CH_3)_3$ deposition. (b) Relative energy during the decomposition of one CH_3 from $Ga(CH_3)_3$ onto surface O atom.

Fig. 4a also illustrates the relative energy with the distance between Ga and the surface during $Ga(CH_3)_3$ deposition. Upon attaining a specific position where the bond energy between the Ga atom and O atoms is strong enough to form bonds, one of the three methyl groups in $Ga(CH_3)_3$ dissociates from the Ga atom and forms a bond with surface O atom. The Ga atom also form bonds with this surface O atom and another one. Because this O atom is simultaneously bonded to Ga atoms and methyl groups, its O–O bond with another surface O atom is broken. The deposition of $Ga(CH_3)_3$ onto the β-Ga_2O_3 surface with only O atoms necessitates surmounting an energy barrier of 0.3 eV.

Furthermore, the energy change associated with the decomposition of one CH_3 in $Ga(CH_3)_3$ onto surf-O is depicted in Fig. 4b. The energy consumed in breaking and forming new bonds during this process is greater than the energy released, resulting in a decrease in relative energy during this process. Thus, the adsorption energy of the reaction process during this process is −4.3716 eV and although there is a relatively small 0.3 eV energy barrier, it is also an exothermic reaction that can occur spontaneously. The negative adsorption energy signifies that the reaction is thermodynamically favorable, given that it releases energy. At the same time, the small energy barrier suggests that the reaction can overcome this activation energy with relative ease, allowing it to occur without the need for an external energy input.

3.3.1 Bonding of two methyl groups. After the deposition of $Ga(CH_3)_3$, we first moved the H atom that is furthest from the Ga atom on the dissociated methyl group to the nearest oxygen atom on the surface. This promotes and simulates the reaction process wherein the methyl group interacts with the surface. Upon reaching the critical position, the C–H bond breaks and the H atom forms a hydroxyl group with the surface O atom. At the same time, we weakened the bond energy between the Ga atom and its associated methyl group by moving the methyl group closer to the dissociated methyl in dimethylgallium towards a direction away from Ga. The process of hydroxyl generation involves bond formation, which is exothermic, accounting for the rapid decrease in relative energy observed during the movement process, as depicted in the structural diagram in Fig. 5a. We then continued to move the CH_3 after the formation of hydroxyl groups. When the methyl shifts to a position sufficiently close to the dissociated methyl, the atomic position constraint is eliminated while the model relaxes. Then, the moved methyl group immediately breaks the Ga–C bond with the Ga atom, forming a bond with the dissociated methyl. Also, owing to the mutual repulsion between atoms, it can be seen in Fig. 5c that both methyl and methyl gallium move away from each other simultaneously during the relaxation process. The relative energy associated with the bonding process of two methyl and the formation of hydroxyl is shown in Fig. 5a and b, where two energy barriers of 1.61 eV and 0.45 eV need to be overcome, respectively.

3.3.2 Generation of the C_2H_4 gas. The second movement is mainly the process of the H atom farthest from the C atom in C_2H_5 moving towards the nearest O atom on the surface. During this movement and bonding process with the surface O atom, the H atom initially forms a bond with two C atoms in C_2H_5, and then moves to form bridging bonds with two O atoms and one C

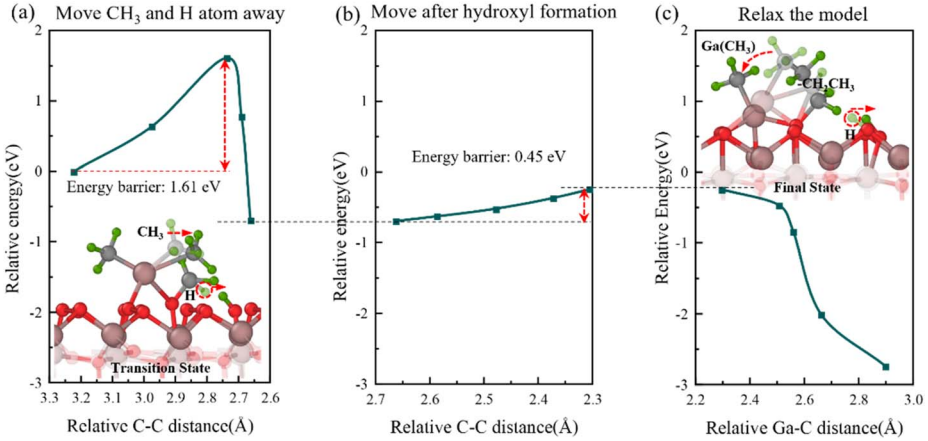

Fig. 5 Semi-transparent and solid structures showing the configurations before and after the reaction step, respectively. Bonding of two methyl groups. (a) Relative energy with distance between C atoms in two shifted methyl groups during the movement of CH_3 and H atoms. (b) Relative energy variation in the process of continuous movement after forming surf − OH. (c) Relative energy during the model relaxation.

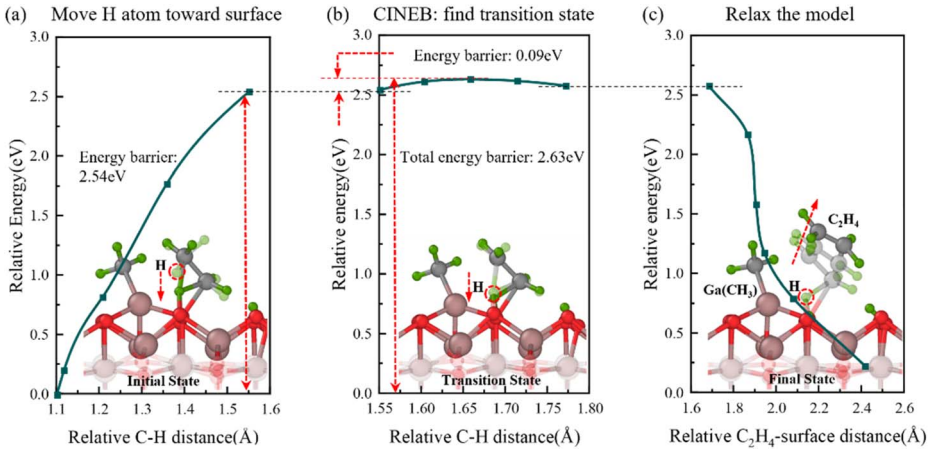

Fig. 6 Semi-transparent and solid structures showing the configurations before and after the reaction step, respectively. The generation of C_2H_4 gas. (a) Relative energy with distance between the moved methyl H atom and its C atom during the movement of H atom toward surface O atom. (b) Relative energy variation in the CINEB process to find the transition state. (c) Relative energy during the model relaxation.

atom in C_2H_5. Fig. 6a and b illustrate the relative energy with the C–H distance during the second move, where the barrier energy is 2.63 eV. Upon relaxation of the model and release of atomic constraints, C_2H_5 breaks the C–H bond with H atom and it also breaks the O–C bond with the surface, resulting in the formation of C_2H_4 gas.

Trimethylgallium is deposited onto the β-Ga_2O_3 surface with only O atoms, and subsequently undergoes a reaction to form methyl gallium and two hydroxyl groups on surface after two moves. The presence of H atoms in two hydroxyl groups is similar to the surface of hydrogen-terminated gallium oxide, where the H atom exists in two distinct forms within hydroxyl groups, *i.e.*, as O–H in one group, and as O–H–O in another. Thus, the deposited trimethyl gallium can react with the hydroxyl groups produced after the reaction. Furthermore, methyl gallium is a reactant of reaction B, and thus this reaction can not only promote the reaction rate of reaction A, but also facilitate the occurrence of reaction B.

The above-mentioned two reaction processes are both trimethylgallium deposition processes, providing Ga atoms for the growth of gallium oxide. After blowing away the remaining unreacted precursor trimethylgallium and other products through an inert carrier gas, we assume that the hydroxyl group reaction on the surface of A is complete, leaving only methyl gallium for the subsequent oxidation reaction. In the following reaction B, the entry of O_2 into the system to participate in the reaction provides an O source for the growth of β-Ga_2O_3.

3.4 Oxidation process following deposition process

We used β-Ga_2O_3 surfaces with two methyl gallium to investigate the mechanism of the oxidation process, and the reaction process between methyl gallium and oxygen can be summarized by chemical reaction (3).

$$2\text{surf} - \text{O} - \text{Ga}(\text{CH}_3) + 2\text{O(g)} \rightarrow 2\text{surf} - \text{O} - \text{Ga} - \text{OH} + \text{C}_2\text{H}_4 \quad (3)$$

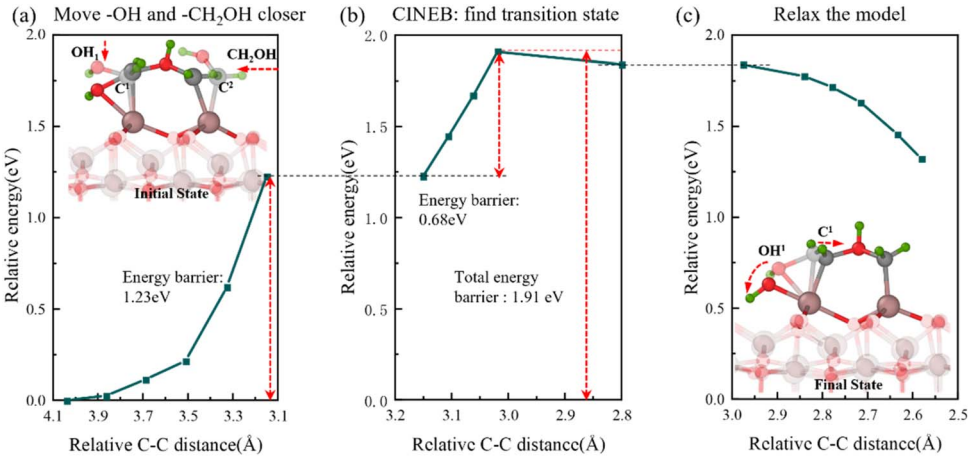

Fig. 7 Semi-transparent and solid structures showing the configurations before and after the reaction step, respectively. Reaction of O atoms with methyl gallium. (a) Relative energy with C–C distance during the movement of –OH and –CH_2OH. (b) Relative energy variation in the CINEB process to find the transition state. (c) Relative energy during the model relaxation.

3.4.1 Generation of the OH on methyl. When O_2 enters the system and reacts with methyl gallium on the surface, an O atom is inserted between an H atom and C atom in a methyl group, forming a hydroxyl group on methyl. The two –CH_2OH are generated as shown in the transparent structure in Fig. 7a. To facilitate the reaction between methyl groups, we moved one hydroxyl of the methyl to the nearest Ga atom, while moving the other CH_2OH towards this methyl. Then the OH_1 bond with both a Ga atom and C^1 atom, as well as the O atom in –CH_2OH bond with the C^1 atom. Furthermore, employing the NBE method can identify the transition states during the relocation process, as shown in Fig. 7b. Also, Fig. 7a and b show the relative energy and distance between two C atoms during the entire process of movement, respectively, and the total energy barrier of the reaction of O atoms with methyl gallium is 1.9 eV. After relaxing the model, the C–O bond between C^1 and OH_1 is broken. This structure can be seen in the reaction surface in Fig. 7c, where the hydroxyl group is transferred from the methyl group to the Ga atom.

3.4.2 Generation of the C_2H_4 gas. To bond two C atoms to form C_2H_4, which can remove C atoms from the system, we moved the two methylene groups(CH_2) towards each other. Fig. 8a illustrates the relative energy with C–C distance during moving, where the energy barrier is 1.05 eV. Subsequently, we shifted the hydroxyl group between the two carbon atoms towards the gallium atom, which is not yet connected to the hydroxyl group. The relative energy with the distance between the C atom and the O atom of the hydroxyl during moving is shown in Fig. 8b. It is noteworthy that the energy barrier of this motion is 0.78 eV, and thus, the total energy barrier that needs to be overcome throughout the reaction process is 1.83 eV.

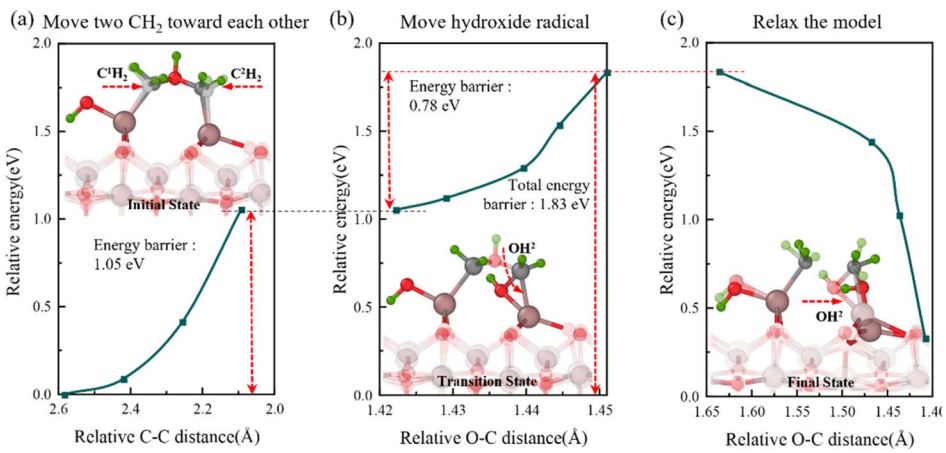

Fig. 8 Semi-transparent and solid structures showing the configurations before and after the reaction step, respectively. First movement during the oxidation process. (a) Relative energy with C–C distance during the movement of two CH_2 groups toward each other. (b) Relative energy with O–C distance during the movement of the hydroxyl group. (c) Relative energy during the model relaxation.

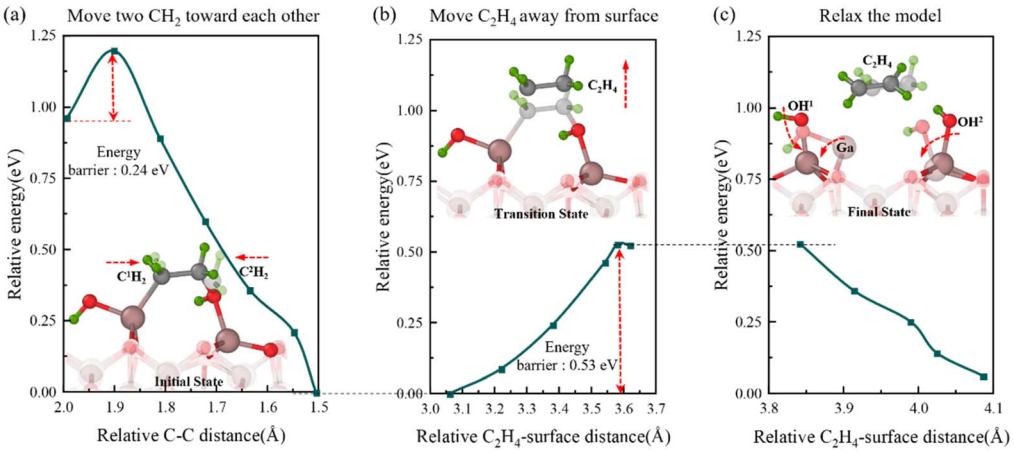

Fig. 9 Semi-transparent and solid structures showing the configurations before and after the reaction step, respectively. Second movement during the oxidation process. (a) Relative energy with C–C distance during the movement of two CH_2 toward each other. (b) Relative energy with C_2H_4-surface distance during the movement of C_2H_4. (c) Relative energy during the model relaxation.

After moving to a certain position, the Ga–C bond breaks and the O atom forms a bond with Ga, ultimately forming a structure of surf-Ga–OH–CH_2. The energy change in the system during this relaxation process and the final structure are shown in Fig. 8c.

After the above-mentioned reaction, there are no other atoms between the two C atoms, but the two C atoms are not bonded. Therefore, we initially shifted the two CH_2 groups towards each other, and Fig. 9a shows the relative energy with C–C distance during this move. The initial movement process requires overcoming a small energy barrier of 0.24 eV. When the two C atoms are close enough, the subsequent reduction in relative energy throughout the followed movement process is attributed to the exothermic characteristics of the C–C bond formation process.

Then, when two C atoms are bonded, we move the entire C_2H_4 upwards until it breaks the C–O and C–Ga bonds. The relative energy change with Ca–C distance during moving C_2H_4 is shown Fig. 9c, where it can be found that it needs overcome an energy barrier of 0.53 eV to break these bonds to form C_2H_4 gas. Finally, we relaxed the model, during which the system evolves into an equilibrium state with reduced energy. According to the structural diagram in Fig. 9c, we can also see that the C_2H_4 gas takes away the C atom and leaves hydroxyl groups on the surface when leaving the system.

After the oxidation reaction, the remaining precursor and reaction byproducts are blown away by inert carrier gas, leaving only hydroxyl groups on the reaction surface. The O atom remains in the system in the form of a hydroxyl group, while the Ga atom has already been added to the model through the deposition process. According to the overall diagram of the growth reaction of gallium oxide shown in Fig. 1, it can be seen that the hydroxyl group generated after the oxidation reaction (reaction B) is the reactant of trimethyl deposition (reaction A), and the methyl gallium produced during the deposition process is also a reactant of the oxidation reaction, thereby establishing an ALD cycle. This allows the continuous growth of gallium oxide through this recurring reaction cycle.

4. Conclusion

In this study, we investigated the growth process of β-Ga_2O_3 using $Ga(CH_3)_3$ and O_2 as Ga and O sources using DFT, respectively, revealing the reaction mechanism involved in the reaction process. We employed the climbing image nudged elastic band method to interpolate between the initial and final states of the reaction, thereby optimizing the entire reaction pathway and calculating the energy barrier of individual reaction processes using this method.

During the first reaction of $Ga(CH_3)_3$ depositing onto the hydrogen-terminated β-Ga_2O_3 surface, two of the three methyl groups move away from the Ga atom and attract surface H atoms to form CH_4 gas. Therefore, the Ga atoms are captured by O atoms in the form of methyl gallium. When $Ga(CH_3)_3$ is subsequently deposited onto the surface of gallium oxide after H atoms have been consumed, one methyl group is decomposed onto the surface-O. Also, one of the other two methyl groups is attracted by this methyl group, thus moving away from the Ga atom and bonding with it. The H atoms on the two bonded methyl groups are attracted by the surface O atoms, generating C_2H_4 gas and leaving the system. After the deposition process, which a layer of Ga atoms is added on the surface of the model in the form of the product methyl gallium, we subsequently employed inert gas blowing to meticulously remove any residual precursors or by-products that may have adhered to the surface. Then, O_2 only reacts with methyl groups during the oxidation process, and the H atoms in the methyl groups and O atoms form hydroxyl groups, which are captured by the Ga atom. The carbon atoms in the two methyl groups attract each other, forming a C–C bond and producing C_2H_4 gas, which leaves the system. This oxidation process results in the formation of an O atomic layer on the surface of the model.

Consequently, the β-Ga_2O_3 thin film can be produced by repeating the deposition and oxidation process.

The calculation results in this work not only provide some insights into the growth of a β-Ga_2O_3 layer on the surface of hydrogen-terminated β-Ga_2O_3 (100), providing the corresponding parameters for multi-scale simulation in subsequent work, and simulate and analyze at higher time and spatial scales, but also provide impetus for further theoretical and experimental research.

Conflicts of interest

The authors declare that they have no conflict of interest.

Data availability

The data that support the findings of this study are available within the article and its supplementary information (SI). Supplementary information: The SI for this article includes: the optimized geometries of every transition state invoked in the proposed mechanism. See DOI: **https://doi.org/10.1039/d5ra05380c**.

Acknowledgements

This work is supported by the National Science Foundation of China under Grant No. 12172112, 52293372, 11932005, and 11974091 and the National Natural Science Foundation of China (Joint Fund for Corporate Innovation and Development – Key Program) Grant no. U22B2082.

References

1 X. Hou, Y. Zou, M. Ding, Y. Qin, Z. Zhang, X. Ma, P. Tan, S. Yu, X. Zhou, X. Zhao, G. Xu, H. Sun and S. Long, *J. Phys. D: Appl. Phys.*, 2021, **54**, 043001.
2 H. Y. Playford, A. C. Hannon, E. R. Barney and R. I. Walton, *Chem. Eur J.*, 2013, **19**, 2803–2813.
3 J. W. Roberts, J. C. Jarman, D. N. Johnstone, P. A. Midgley, P. R. Chalker, R. A. Oliver and F. C.-P. Massabuau, *J. Cryst. Growth*, 2018, **487**, 23–27.
4 S. H. Lee, K. M. Lee, Y.-B. Kim, Y.-J. Moon, S. B. Kim, D. Bae, T. J. Kim, Y. D. Kim, S.-K. Kim and S. W. Lee, *J. Alloys Compd.*, 2019, **780**, 400–407.
5 L. Gu, H.-P. Ma, Y. Li, A.-F. Wang, W.-J. Chen, Z.-R. Tang, Y. Shen, F. Y. Sun, J.-T. Zhu and Q.-C. Zhang, *Appl. Surf. Sci.*, 2023, **641**, 158502.
6 S. Raghuvansy, J. P. McCandless, M. Schowalter, A. Karg, M. Alonso-Orts, M. S. Williams, C. Tessarek, S. Figge, K. Nomoto, H. G. Xing, D. G. Schlom, A. Rosenauer, D. Jena, M. Eickhoff and P. Vogt, *APL Mater.*, 2023, **11**, 111113.
7 H. Hayashi, R. Huang, H. Ikeno, F. Oba, S. Yoshioka, I. Tanaka and S. Sonoda, *Appl. Phys. Lett.*, 2006, **89**, 181903.
8 T. Kato, H. Nishinaka, K. Shimazoe, K. Kanegae and M. Yoshimoto, *ACS Appl. Electron. Mater.*, 2023, **5**, 1715–1720.
9 Z. Chen, Z. Li, Y. Zhuo, W. Chen, X. Ma, Y. Pei and G. Wang, *Appl. Phys. Express*, 2018, **11**, 101101.
10 F. Boschi, M. Bosi, T. Berzina, E. Buffagni, C. Ferrari and R. Fornari, *J. Cryst. Growth*, 2016, **443**, 25–30.
11 S. J. Pearton, J. Yang, P. H. Cary IV, F. Ren, J. Kim, M. J. Tadjer and M. A. Mastro, *Appl. Phys. Rev.*, 2018, **5**, 011301.
12 R. Roy, V. G. Hill and E. F. Osburn, *Chem. Soc.*, 1952, **74**, 719–722.
13 Y. Ma, B. Feng, X. Zhang, T. Chen, W. Tang, L. Zhang, T. He, X. Zhou, X. Wei, H. Fu, K. Xu, S. Ding and B. Zhang, *Vacuum*, 2021, **191**, 110402.
14 M. Higashiwaki, *AAPPS Bull.*, 2022, **32**, 3.
15 Z. Galazka, *Semicond. Sci. Technol.*, 2018, **33**, 113001.
16 J. Qu, S. C. E. Tsang and X.-Q. Gong, *J. Mol. Model.*, 2014, **20**, 2543.
17 M. Yamamoto, A. Kuwabara and T. Yoshida, *ACS Omega*, 2021, **6**, 33701–33707.
18 F. Alema, B. Hertog, A. Osinsky, P. Mukhopadhyay, M. Toporkov and W. V. Schoenfeld, *J. Cryst. Growth*, 2017, **475**, 77–82.
19 H. Murakami, K. Nomura, K. Goto, K. Sasaki, K. Kawara, Q. T. Thieu, R. Togashi, Y. Kumaghi, M. Higashiwaki and A. Kuramata, *Appl. Phys. Express*, 2015, **8**, 015503.
20 K. Sasaki, A. Kuramata, T. Masui, E. G. Víllora, K. Shimamura and S. Yamakoshi, *Appl. Phys. Express*, 2012, **5**, 5502.
21 X. Liu, F. Ma, S. Wang, L. He, Y. Jia, Q. Lu, H. Chen and Y. Hao, *J. Mater. Chem. C*, 2022, **10**, 16247.
22 S. Ilhom, A. Mohammad, J. Grasso, B. G. Willis, A. K. Okyay and N. Biyikli, *ACS Appl. Electron. Mater.*, 2023, **5**, 335–343.
23 Y. Yang, X.-Y. Zhang, C. Wang, F.-B. Ren, R.-F. Zhu, C.-H. Hsu, W.-Y. Wu, D.-S. Wuu, P. Gao, Y.-J. Ruan, S.-Y. Lien and W.-Z. Zhu, *Nanomaterials*, 2022, **12**, 1510.
24 A. Mahmoodinezhad, C. Janowitz, F. Naumann, P. Plate, H. Gargouri, K. Henkel, D. Schmeißer, J. I. Flege and J. Vac, *Sci. Technol. A*, 2020, **38**, 022404.
25 V. D. Wheeler, N. Nepal, D. R. Boris, S. B. Qadri, L. O. Nyakiti, A. Lang, A. Koehler, G. Foster, S. G. Walton, C. R. Eddy Jr and D. J. Meyer, *Chem. Mater.*, 2020, **32**, 1140–1152.
26 W. Liu, J. He, X. Zhu, T. Huang, X. Chen, Y. Zheng, L. Chen and R. Zhang, *Thin Solid Films*, 2023, **766**, 139655.
27 X. Li, H.-L. Lu, H.-P. Ma, J.-G. Yang, J.-X. Chen, W. Huang, Q. Guo, J.-J. Feng and D. W. Zhang, *Curr. Appl. Phys.*, 2019, **19**, 72–81.
28 R. K. Ramachandran, J. Dendooven, J. Botterman, S. P. Sree, D. Poelman, J. A. Martens, H. Poelman and C. Detavernier, *J. Mater. Chem. A*, 2014, **2**, 19232–19238.
29 S.-Y. Chu, M.-X. Shen, T.-H. Yeh, C.-H. Chen, C.-T. Lee and H.-Y. Lee, *Sensors*, 2020, **20**, 6159.
30 M. K. Akbari, N. S. Lopa and S. Zhuiykov, *Coatings*, 2023, **13**, 1041.
31 H. Altuntas, I. Donmez, C. Ozgit-Akgun and N. Biyikli, *J. Vac. Sci. Technol., A*, 2014, **32**, 041504.
32 S. D. Elliott, G. Dey, Y. Maimaiti, H. Ablat, E. A. Filatova and G. N. Fomengia, *Adv. Mater.*, 2015, **28**, 5367–5380.

33 W. Feng, S. Chen, Z. Lin, Z. Chen, G. Wang, X. Chen and Y. Pei, *J. Alloys Compd.*, 2023, **951**, 169793.
34 J. Kwon, M. Dai, M. D. Halls and Y. J. Chabal, *Chem. Mater.*, 2008, **20**, 3248–3250.
35 G. Prechtl, M. Kersch, G. S. Icking-Konert, W. Jacobs, T. Hecht, H. Boubekeur and U. Schröder, *IEEE International Electron Devices Meeting Technical Digest*, 2003, 245–248.
36 S. D. Elliott, G. Scarel, C. Wiemer, M. Fanciulli and G. Pavia, *Chem. Mater.*, 2006, **18**, 3764–3773.
37 R. L. Puurunen, *J. Appl. Phys.*, 2005, **97**, 121301.
38 K. A. Hatch, D. C. Messina and R. J. Nemanich, *J. Vac. Sci. Technol., A*, 2022, **40**, 042603.
39 D. J. Comstock and J. W. Elam, *Chem. Mater.*, 2012, **24**, 4011–4018.
40 L. Aarik, H. Mändar, J. Kozlova, A. Tarre and J. Aarik, *Cryst. Growth Des.*, 2023, **23**, 5899–5911.
41 S. Ilhom, A. Mohammad, J. Grasso, B. G. Willis, A. K. Okyay and N. Biyikli, *ACS Appl. Electron. Mater.*, 2023, **5**, 335–343.
42 V. M. Bermudez, *Chem. Phys.*, 2006, **323**, 193–203.
43 G. Kresse and J. Furthmüller, *Phys. Rev. B:Condens. Matter Mater. Phys.*, 1996, **54**, 11169.
44 G. Kresse and J. Furthmüller, *Comput. Mater. Sci.*, 1996, **6**, 15–50.
45 J. P. Perdew, K. Burke and M. Ernzerhof, *Phys. Rev. Lett.*, 1996, **77**, 3865–3868.
46 P. E. Blöchl, *Phys. Rev. B:Condens. Matter Mater. Phys.*, 1994, **50**, 17953.
47 G. Kresse and D. Joubert, *Phys. Rev. B:Condens. Matter Mater. Phys.*, 1999, **59**, 1758–1775.
48 H. Jónsson, G. Mills and K. W. Jacobsen, *World Sci.*, 1998, 385–404.
49 G. Henkelman, B. P. Uberuaga and H. Jónsson, *J. Chem. Phys.*, 2000, **113**, 9901–9904.
50 J. Su, R. Guo, Z. Lin, S. Zhang, J. Zhang, J. Chang and Y. Hao, *J. Phys. Chem. C*, 2018, **122**, 24592–24599.